Article

The Effects of Different Blending Methods on the Thermal, Mechanical, and Optical Properties of PMMA/SiO$_2$ Composites

Chi-Kai Lin [1,†], Jia-Wei Xie [1,†], Ping-Jui Tsai [2,*], Hao-Yu Wang [1], Zhi-Wei Lu [1], Tung-Yi Lin [3,4,*] and Chih-Yu Kuo [1,5,*]

1 Department of Chemical Engineering and Biotechnology, National Taipei University of Technology, Taipei 106, Taiwan
2 Bone and Joint Research Center, Chang Gung Memorial Hospital, Linkou 333, Taiwan
3 Institute of Polymer Science and Engineering, National Taiwan University, Taipei 106, Taiwan
4 Department of Orthopedic Surgery, Chang Gung Memorial Hospital Keelung Branch and Chang Gung University, Taoyuan 333, Taiwan
5 High-Value Biomaterials Research and Commercialization Center, National Taipei University of Technology, Taipei 106, Taiwan
* Correspondence: brett1130@gmail.com (P.-J.T.); ross_1222@hotmail.com (T.-Y.L.); chihyukuo@ntut.edu.tw (C.-Y.K.)
† These authors contributed equally to this work.

Abstract: In this study, PMMA/SiO$_2$ composites were fabricated with monodispersed SiO$_2$ and PMMA using four distinct methods—physical blending, in situ polymerization, random copolymerization, and block copolymerization—to investigate the composites' thermal, mechanical, and optical properties. In the physical blending approach, SiO$_2$ nanoparticles were dispersed in a PMMA solution, while during in situ polymerization, silica nanoparticles were incorporated during the synthesis of PMMA/SiO$_2$ composites. 3-methacryloxypropyltrimethoxysilane (MPS) was modified on the SiO$_2$ surface to introduce the reactive double bonds. The MPS@SiO$_2$ was either random- or block-copolymerized with PMMA through RAFT polymerization. The PMMA/SiO$_2$ composites prepared via these different methods were characterized using FTIR, TGA, and DSC to determine their chemical structures, thermal degradation temperatures, and glass transition temperatures, respectively. Scanning electron microscopy (SEM) was employed to observe the microstructures and dispersion of the composites. This comprehensive analysis revealed that the PMMA/SiO$_2$ composites prepared via block copolymerization exhibited thermal stability at temperatures between 200 and 300 °C. Additionally, they demonstrated excellent transparency (86%) and scratch resistance ($\geq$6H) while maintaining mechanical strength, suggesting their potential application in thermal insulation materials.

Keywords: RAFT polymerization; SiO$_2$; PMMA; organic/inorganic composites

1. Introduction

Composite materials are formed by combining two or more materials through physical or chemical methods [1], typically involving a matrix material and one or more fillers [2]. Fillers play an important role in many fields, including thermal, electrical, tribological, and mechanical properties [2,3]. Among these properties, mechanical property enhancement received attention for polymeric composites since polymers are considered to lack mechanical tolerance. For example, carbon fiber fillers can effectively increase the strength and stiffness of composite materials [4] while also improving heat and corrosion resistance [5–7]. Glass fibers also offer high strength and stiffness, though they are more brittle and prone to fracture compared to carbon fibers [8,9]. Ceramics have extremely high hardness and wear resistance but are easily broken and not resistant to vibrations and thermal cycling [10,11]. The size and mixing method of the filler also influences the properties of composites [12–15].

Small particles possess a large surface energy, resulting in severe self-aggregation. Therefore, the dispersion of nanoparticles in the polymer matrix is difficult [16]. Excessive or uneven particle sizes can lead to anisotropy in the composite, impacting its mechanical properties. Thus, particles influence the strength of polymer composites in two distinct ways. One is the weakening effect caused by stress concentration, while the other is the strengthening effect, as these particles may act as barriers to crack propagation within the composites [17]. When the weakening effect predominates, the mechanical strength of the composite will be inferior to that of the matrix. Conversely, when the strengthening effect is more pronounced, the strength of composites is enhanced. Among the hard particles, silica particles have many advantages as filler candidates, including cost-effectiveness, good dispersibility, and mechanical strength [18–21]. In terms of thermal properties, silica also performs excellently as a reinforcing material, improving the thermal stability of composites and maintaining good stability in high-temperature environments. For example, Far et al. mixed the binary carbonate, Li_2CO_3-K_2CO_3, with SiO_2 nanoparticles, and this was shown to increase the heat capacity by 19% [22].

The advantage of thermoplastics polymers lies in their malleability, enabling the creation of intricate shapes through processes such as thermoforming, injection molding, and 3D printing [23,24]. However, their heat and chemical resistance are generally inferior. The curing process of thermosetting materials is an irreversible chemical reaction, during which chemical bonds form between polymer molecules to create a 3D network structure [25]. This network structure gives thermosetting polymers excellent heat, chemical, and wear resistance. Thermoplastic materials, on the other hand, have reversible thermal deformation characteristics, allowing them to be reshaped multiple times through heating and cooling to produce complex shapes. However, their heat and chemical resistance are generally poor, necessitating the addition of fillers to enhance their properties [26]. Among the many thermoplastic materials, polymethyl methacrylate (PMMA) has high transparency and good optical transmittance, meaning it is commonly used to manufacture transparent products such as optical lenses and display panels. PMMA is also frequently used in the medical field, such as in dental materials and bone cements [27–29].

Therefore, the present study attempts to primarily use SiO_2 nanoparticles and PMMA as the main materials to assess the preparation and properties of organic/inorganic composites. The Stöber method was first used to synthesize SiO_2. 3-methacryloxypropyltrimethoxysilane (MPS) was then used to modify the surface with reactive unsaturated double bonds (MPS@SiO_2), allowing it to copolymerize with methyl methacrylate monomers [30]. Four different methods—the physical blending of SiO_2 and PMMA, the in situ polymerization of SiO_2 with MMA, and the random and block copolymerization of MPS@SiO_2 with MMA—were utilized to prepare blended PMMA/SiO_2, in situ PMMA/SiO_2, PMMA-*co*-SiO_2, and PMMA-*b*-SiO_2. FTIR, TGA, DSC, mechanical studies, scratch resistance, and transparency methods were adapted for analyzing the properties of PMMA/SiO_2 composites. To the best of our knowledge, this is the first study that compares four different methods for preparing PMMA/SiO_2 composites. It is believed that this study can benefit the synthesis of not only PMMA/SiO_2 but also various other composites.

2. Experimental

2.1. Materials

Tetraethyl orthosilicate (TEOS) was purchased from Thermo Scientific. 3-methacryloxypropyl trimethoxysilane (MPS), methyl methacrylate (MMA), 2,2-Azobis(2-methylpropionitrile) (AIBN), and ammonium peroxydisulfate (APS) were purchased from Alfa, Linkou, Taiwan. The 35% Ammonia solution was purchased from Fisher, while the CTA, 4-cyano-4-(phenylcarbonothioylthio)pentanoic acid (CPDB) was purchased from Sigma Aldrich, Linkou, Taiwan. All chemical reagents are used directly as received without further purification.

2.2. Synthesis of the SiO$_2$ and MPS@SiO$_2$ Nanoparticles

In this experiment, 63.32 mL ethanol, 1.82 mL ammonia, 0.4 g deionized water, and 8.5 mL TEOS were stirred together and reacted at 40 °C for 50 min. The solution was then dried using a rotary evaporator to obtain solid particles as monodispersed SiO$_2$. MPS@SiO$_2$ was synthesized similarly to SiO$_2$ with MPS added during the reaction.

2.3. Synthesis of Pristine PMMA, PMMA/SiO$_2$ Composites with Different Methods

<u>PMMA</u>: In this step, 60 mL deionized water, 40 mL acetone, 8.6 mL MMA monomer, and 0.2 g APS initiator were added to a three-neck flask. The reaction was carried out at 75 °C for 24 h. The sample was purified using a rotary evaporator for later use.

The PMMA/SiO$_2$ composite was synthesized using four different methods. The feeding amount of SiO$_2$ to PMMA was set as 5 wt. % for the four methods.

<u>Blending</u>: The purified PMMA was dissolved in acetone. Then, 17.2 mL SiO$_2$ solution was added and mixed uniformly, and it was dried overnight at 50 °C to obtain blended PMMA/SiO$_2$ powder.

<u>In situ polymerization</u>: In this step, 60 mL deionized water, 40 mL acetone, 8.6 mL MMA monomer, and 17.2 mL SiO$_2$ solution were added to a three-neck flask, and 0.2 g APS initiator was added. The reaction was carried out at 75 °C for 24 h. The sample was purified using a rotary evaporator to obtain in situ PMMA/SiO$_2$ powder.

<u>RAFT copolymerization</u>: In this step, 100 mL ethanol, 0.48 g CPDB, 0.06 g AIBN, 17.2 mL MMA, and 32.4 mL MPS@SiO$_2$ solution were added to a three-neck flask and mixed uniformly. The reaction was carried out at 70 °C under nitrogen for 40 h. The sample was purified using a rotary evaporator to obtain PMMA-*co*-SiO$_2$.

<u>RAFT block copolymerization</u>: In this step, 100 mL ethanol, 0.48 g CPDB, 0.06 g AIBN and 17.2 mL MMA were added together and reacted at 70 °C under nitrogen for 24 h. Then, 32.4 mL MPS@SiO$_2$ solution was added, and the reaction continued for 16 h under nitrogen. The sample was purified using a rotary evaporator to obtain PMMA-*b*-SiO$_2$.

2.4. Structural Characterization of the PMMA/SiO$_2$ Composites

A thermogravimetric analysis (TGA, Pyris 1 TGA) was used to determine the thermal decomposition of PMMA/SiO$_2$ composites. The samples were heated from 50 °C to 700 °C with a heating rate of 20 °C/min, and the N$_2$ flow rate was maintained at 20 mL/min. The glass transition temperatures (Tgs) of as-synthesized PMMA/SiO$_2$ composites were determined using a differential scanning calorimeter (DSC, NETZSCH DSC 200F3) at a heating rate of 20 °C/min. The Tgs were then determined using the second heating curves. Fourier transform infrared spectroscopy (FTIR, HORIBA v FT-IR Spectrometer) absorption spectra were measured at frequencies ranging from 4000 to 400 cm^{-1} with a 4 cm^{-1} resolution. The samples were mixed with KBr and prepared as pellets.
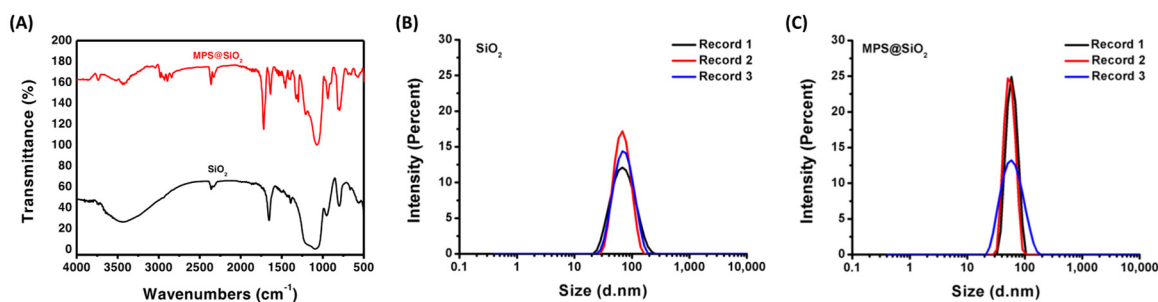
2.5. Mechanical and Morphology of PMMA/SiO$_2$ Composites

To analyze the mechanical properties, PMMA/SiO$_2$ composites were first dispersed in acetone and then poured into a Teflon mold (ISO-37 dumbbell-shaped type 3). A universal material testing machine (YM-H3501-A02) was used to determine the Young's modulus, yield strength, fracture strength, and maximum elongation of PMMA/SiO$_2$ composites. The surface and structural morphologies of PMMA/SiO$_2$ composites were studied using SEM (JEOL JSM-7610F) images. The scratch resistance (pencil hardness) of PMMA/SiO$_2$ composite films was analyzed using a commercial pencil hardness tester (scratch hardness tester model 291, ERICHSEN test equipment). This test conforms to ASTM standard D3363, and involves different hardness grades (9B–9H) to evaluate the scratch resistance of PMMA/SiO$_2$ composite films. The transparency of PMMA/SiO$_2$ composite films was determined via a UV/Vis transmittance analysis in the range of 400–750 nm.

3. Results and Discussion

3.1. Characterization of SiO₂ and MPS@SiO₂ Nanoparticles

The functional groups and particle sizes on the SiO_2 surface before and after MPS modification were determined via FTIR and DLS. The absorption peaks at 466 cm^{-1} and 802 cm^{-1} correspond to the bending and symmetric stretching vibrations of the Si–O–Si bonds, as shown in Figure 1A. The peak at 1095 cm^{-1} represents the asymmetric stretching vibration of the Si–O–Si bond. A broad characteristic peak at 3463 cm^{-1} is attributed to the stretching vibration of hydroxyl groups on the SiO_2 surface, which is responsible for reacting with the vinyl groups of the silane coupling agent MPS. After surface modification, new peaks appear at 1635, 1299, and 937 cm^{-1} for MPS@SiO₂, representing the C=C stretching vibrations, C–O stretching vibrations, and Si–O–C stretching vibrations of MPS, respectively. Furthermore, the original hydroxyl peak at 3463 cm^{-1} was reduced, confirming the successful grafting of MPS onto the SiO_2 surface, replacing the surface hydroxyl groups. Figure 1B,C depict the particle size distribution of SiO_2 and MPS@SiO₂. The results show that the average particle size of SiO_2 is 60.75 nm, with a polydispersity index (PDI) of 0.095, indicating a uniform distribution. After modifying the SiO_2 surface with MPS, the average particle size increased from 65 nm to 85 nm, and the polydispersity index slightly increased to 0.33.
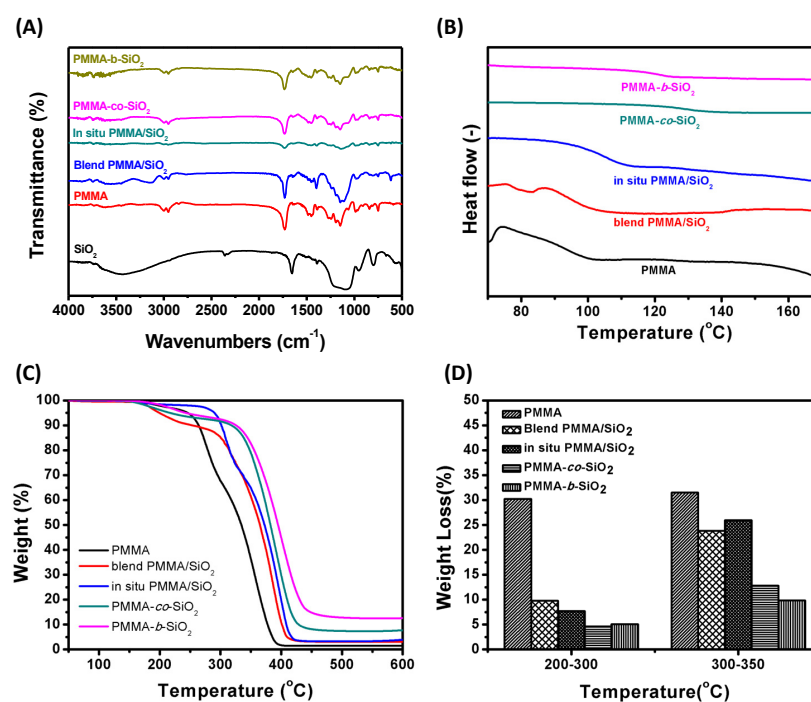

Figure 1. (**A**) FTIR analysis of SiO_2 and MPS@SiO₂; DLS analysis of (**B**) SiO_2 and (**C**) MPS@SiO₂.

3.2. Characterization of the PMMA/SiO₂ Composites

The results of FTIR analyses of PMMA, SiO_2, and PMMA/SiO₂ composites are shown in Figure 2A, which allows us to determine the interaction between the PMMA and SiO_2 nanoparticles. The peak at 1731 cm^{-1} corresponds to the stretching of the carbonyl groups in PMMA. The peaks at 1454 cm^{-1} and 1392 cm^{-1} are attributed to the -CH stretching of PMMA, with 1454 cm^{-1} corresponding to the methyl group (-C<u>H</u>$_3$) and 1392 cm^{-1} to the methylene group (-C<u>H</u>$_2$-). After introducing SiO_2 nanoparticles, all PMMA/SiO₂ composites exhibit a characteristic peak at 1110 cm^{-1}, belonging to the Si–O–Si bond, indicating the successful incorporation of SiO_2. Additionally, the characteristic peak at 1643 cm^{-1} of PMMA-*co*-SiO₂ and PMMA-*b*-SiO₂ confirms the introduction of MPS@SiO₂. On the other hand, blend PMMA/SiO₂ leads to a stronger intensity in the characteristic spectral peaks than in situ PMMA/SiO₂, PMMA-*co*-SiO₂, and PMMA-*b*-SiO₂. This indicates a sufficient SiO_2 content in blend PMMA/SiO₂ than in other PMMA/SiO₂ composites. The glass transition temperatures (Tgs) of PMMA, blend PMMA/SiO₂, in situ PMMA/SiO₂, PMMA-*co*-SiO₂, and PMMA-*b*-SiO₂ are 101 °C, 102 °C, 109 °C, 131 °C, and 126 °C, as shown in the DSC analysis (Figure 2B). The physical introduction of SiO_2 does not significantly affect the Tgs of PMMA/SiO₂ composites due to the absence of chemical bonding. However, SiO_2 is integrated into the polymer backbone through polymerization, effectively enhancing the Tgs of PMMA/SiO₂ composites. Figure 2C shows a comparison of the thermal weight losses of PMMA and PMMA/SiO₂ composites at different temperatures. It is obvious that there are three distinct thermal decomposition stages for PMMA (Figure 2C). The first stage is observed between 165 °C and 250 °C with 6.38 wt. % weight loss attributed to the depolymerization initiated from head-to-head linkage within the polymer chain [31,32]. The second stage occurs between 250 °C and 300 °C with 26.41 wt. % weight loss resulting

from the thermal decomposition of the unsaturated chain ends. Above 300 °C, breaking and decomposition among the PMMA backbone occurs, leading to the most significant weight loss. The thermal decomposition of blende PMMA/SiO$_2$ is relatively lower in the range of 200 °C to 300 °C (Figure 2D), indicating that the unsaturated chain ends do not affect the weight loss resulting from the SiO$_2$ protection layer, thereby enhancing the thermal stability [33]. The in situ PMMA/SiO$_2$ followed the same trend as PMMA, but the two thermal decomposition peaks were delayed from 250 °C and 300 °C to 280 °C and 330 °C, respectively (based on the differential spectrum, unshown). This delay can be attributed to the spatial barrier formed by PMMA-encapsulated SiO$_2$, which acts against the heat transfer path and slows heat transfer [34,35]. A 3 wt. % mass residue can be observed at temperatures above 500 °C, confirming the presence of SiO$_2$ in the blend and in situ PMMA/SiO$_2$ composites. However, from the thermal decomposition (Figure 2C) and differential plots of PMMA-*co*-SiO$_2$ and PMMA-*b*-SiO$_2$, it can be found that the weight loss that originally occurred before the main chain decomposition was not present (165–250 °C). At the same time, the weight loss caused by the thermal decomposition of the unsaturated chain ends was significantly reduced from 28.6 wt. % to below 5 wt. %. This reduction is due to the controlled nature of RAFT polymerization, in which the stable intermediate prevents the termination and avoids the formation of unsaturated chain ends. Thus, the maximum weight loss in PMMA-*co*-SiO$_2$ and PMMA-*b*-SiO$_2$ occurred above 335 °C. Meanwhile, the remaining weights of PMMA-*co*-SiO$_2$ and PMMA-*b*-SiO$_2$ were 7.69% and 12.61% higher than the feeding ratio (5 wt. %) due to the introduction of SiO$_2$ by RAFT polymerization. In short, we can conclude that the thermal stability improves between 200 °C and 300 °C regardless of the method of SiO$_2$ introduction by comparing the relationship between mass loss and temperature, as shown in Figure 2D. The thermal degradation of the PMMA main chain results in a significant weight loss for PMMA, blend PMMA/SiO$_2$, and in situ PMMA/SiO$_2$ beyond 300 °C. However, RAFT polymerization effectively maintains the thermal stability of PMMA/SiO$_2$ composites until 350 °C owing to the better dispersion and chemical bonding, which shows the potential in thermal insulation applications.

Figure 2. Characterization of PMMA and PMMA/SiO$_2$ composites: (**A**) FTIR spectrum, (**B**) DSC analysis, (**C**) TGA analysis, and (**D**) weight loss within specific temperature regions of PMMA, and PMMA/SiO$_2$ composites.

3.3. Mechanical Properties of the PMMA/SiO$_2$ Composites

Effective stress transfer is the most crucial factor in strengthening two-phase composites. Different blend methods lead to different dispersions of silica in the PMMA/SiO$_2$ composites, therefore influencing the results of universal testing. For poorly bonded particles, stress transfer at the particle/polymer interface is inefficient. However, in composites containing well-bonded particles, the incorporation of particles into the polymer results in increased strength. Figure 3 illustrates the stress–strain relationship of PMMA/SiO$_2$ composites, in which the blend PMMA/SiO$_2$ and in situ PMMA/SiO$_2$ are shown to enhance the Young's modulus and yield strength of PMMA/SiO$_2$ composites, while the PMMA-*co*-SiO$_2$ and PMMA-*b*-SiO$_2$ exhibit less pronounced improvements in their strength, as shown in Table 1. It is expected that the introduction of SiO$_2$ nanoparticles can improve the mechanical properties of PMMA/SiO$_2$ composites because of the bridging effect. The preparation of PMMA/SiO$_2$ composites via RAFT copolymerization was expected to effectively bond SiO$_2$ to PMMA and enhance mechanical strength. However, the opposite was observed, as PMMA/SiO$_2$ composites prepared by physical methods, i.e., blend and in situ PMMA/SiO$_2$, exhibited higher strength. It is speculated that the RAFT copolymerization process may have introduced the agglomeration of SiO$_2$ nanoparticles or disrupted the orderly long-chain structure of PMMA, weakening the overall mechanical properties [36]. It is noted that PMMA-*b*-SiO$_2$ shows more strain than other PMMA/SiO$_2$ composites. Since PMMA is inherently a brittle acrylic-based polymer, the combination of a tolerance of higher strain and lower stiffness may also result from the decreased molecular weight of the PMMA matrix.
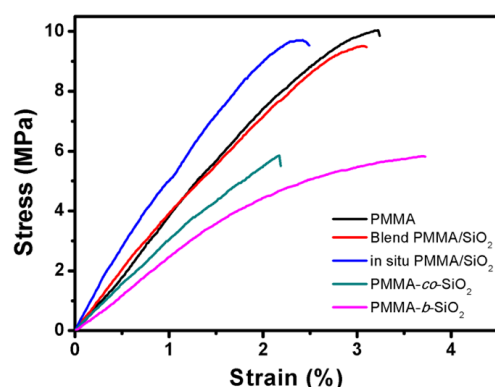

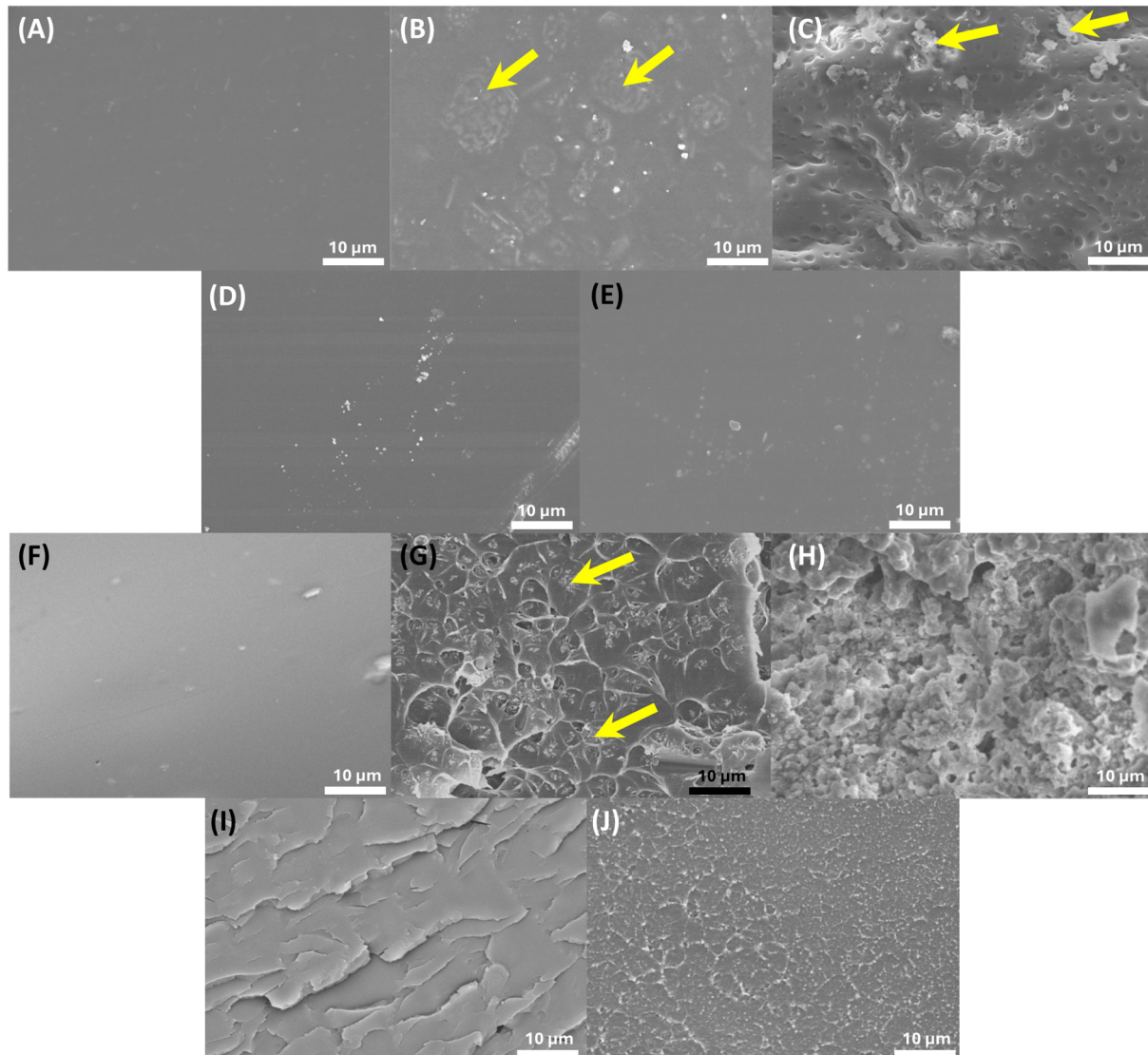**Figure 3.** Tensile stress–strain curves of the PMMA/SiO$_2$ composites prepared by different methods.

Table 1. The mechanical properties of the PMMA/SiO$_2$ composites.

Sample	Young's Modulus (GPa)	Yield Strength (MPa)	Fracture Strength (MPa)	Maximum Elongation (%)
PMMA	0.26 ± 0.18	7.02 ± 4.34	1.92 ± 1.05	3.64 ± 0.01
Blend PMMA/SiO$_2$	0.36 ± 0.02	11.08 ± 2.14	6.11 ± 4.72	4.56 ± 2.05
In situ PMMA/SiO$_2$	0.43 ± 0.06	10.64 ± 3.81	6.81 ± 2.53	3.86 ± 1.71
PMMA-*co*-SiO$_2$	0.25 ± 0.05	4.08 ± 1.98	2.55 ± 0.30	2.89 ± 0.16
PMMA-*b*-SiO$_2$	0.19 ± 0.06	5.33 ± 0.94	1.91 ± 0.61	4.78 ± 0.16

3.4. Morphology of the PMMA/SiO$_2$ Composites

To investigate the relationship between the mechanical properties and morphology of PMMA/SiO$_2$ composites prepared by different methods, thin films of PMMA/SiO$_2$ were fabricated using the solution casting method, and we analyzed the surface and cross-section morphology using SEM images. From the SEM images of PMMA (Figure 4A,F), it can be observed that the PMMA surface was very smooth, while the surface and cross-section structure became uneven with particle aggregation after introducing SiO$_2$ via physical blending or in situ polymerization (Figure 4B,C,G,H). The surface structures of

PMMA-*co*-SiO$_2$ and PMMA-*b*-SiO$_2$ showed slight aggregation but remained relatively smooth (Figure 4D,E). Meanwhile, the cross-section images of PMMA-*co*-SiO$_2$ and PMMA-*b*-SiO$_2$ exhibit a uniform layered structure without aggregation, which suggests that RAFT polymerization provides better thermal stability and more effective dispersion to the PMMA/SiO$_2$ composites compared to physical blending and in situ polymerization.
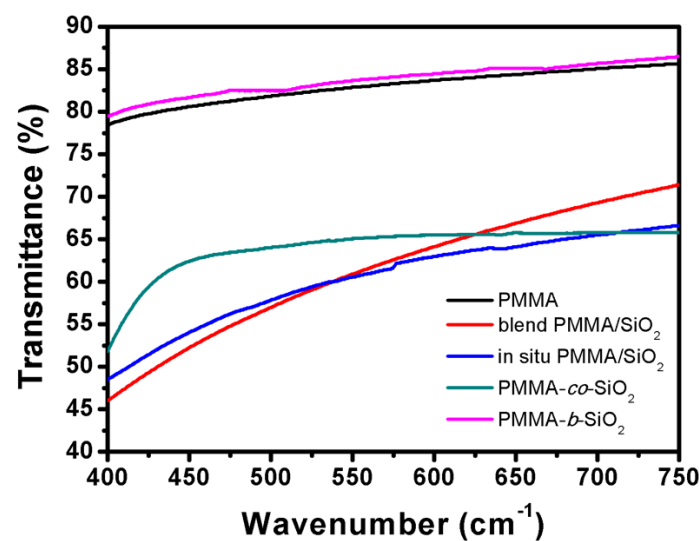

Figure 4. SEM images of the PMMA/SiO$_2$ composites. Surface-area view: (**A**) PMMA, (**B**) blend PMMA/SiO$_2$, (**C**) in situ PMMA/SiO$_2$, (**D**) PMMA-*co*-SiO$_2$, and (**E**) PMMA-*b*-SiO$_2$. Cross-section area view: (**F**) PMMA, (**G**) blend PMMA/SiO$_2$, (**H**) in situ PMMA/SiO$_2$, (**I**) PMMA-*co*-SiO$_2$, and (**J**) PMMA-*b*-SiO$_2$.

The scratch resistance of PMMA/SiO$_2$ composites was measured using a pencil hardness tester, and the results are shown in Table 2. It has been found that pristine PMMA has a scratch resistance of 2H under a 500 g load. Both in situ PMMA/SiO$_2$ and PMMA-*co*-SiO$_2$ showed only minor improvements in scratch resistance, increasing by just one grade to 3H. However, the scratch resistance of blend PMMA/SiO$_2$ was significantly enhanced, reaching a grade of 5H, clearly due to the influence of SiO$_2$. PMMA-*b*-SiO$_2$ demonstrated moderate scratch resistance at 4H, which may be attributed to the RAFT-polymerized composite maintaining structural uniformity. This uniformity, while improving thermal stability, also helps preserve scratch resistance.

Table 2. The scratch resistance of $PMMA/SiO_2$ composites.

Hardness / Sample	2H	3H	4H	5H	6H
PMMA	O	X	X	X	X
Blend $PMMA/SiO_2$	O	O	O	O	X
In situ $PMMA/SiO_2$	O	O	X	X	X
PMMA-*co*-SiO_2	O	O	X	X	X
PMMA-*b*-SiO_2	O	O	O	X	X

PMMA is a polymer with high hardness and transparency; the purpose of our research is to improve its thermal stability but maintain these intrinsic properties after introducing SiO_2 nanoparticles. Figure 5 shows the transmittance of different $PMMA/SiO_2$ composite films prepared via the solution casting method at visible light wavelengths. The maximum transmittance of PMMA is 85.6%, while blend $PMMA/SiO_2$, in situ $PMMA/SiO_2$, PMMA-*co*-SiO_2, and PMMA-*b*-SiO_2 have maximum transmittances of 71.4%, 66.6%, 65.8%, and 86.5%, respectively. It is obvious that after introducing SiO_2 nanoparticles, the transmittance of the blend $PMMA/SiO_2$, in situ $PMMA/SiO_2$, and PMMA-*co*-SiO_2 composites significantly decreased to lower than 70%. Notably, PMMA-*b*-SiO_2 had a minimal impact on the transmittance of PMMA because of the block copolymer structure. The block conformation tends to create the PMMA-rich domain and silica domain. The PMMA-rich domain is dominant, which is similar to pure PMMA, so the transmittance remains.

Figure 5. The visible-light transparency of $PMMA/SiO_2$ composites.

4. Conclusions

We prepared organic/inorganic composite materials ($PMMA/SiO_2$ composites) by incorporating SiO_2 nanoparticles as fillers into PMMA through various blending methods and conducted a series of investigations into their thermal, mechanical, and optical properties. A TGA analysis showed that each blending method effectively improved the thermal properties of PMMA. Physical blending (blend $PMMA/SiO_2$) retained the polymer molecular weight, while in situ $PMMA/SiO_2$ delayed the thermal decomposition temperature by 30 °C due to the steric hindrance provided by SiO_2 nanoparticles. Random (PMMA-*co*-SiO_2) and block copolymerization (PMMA-*b*-SiO_2) reduced the unsaturated chain segments of PMMA, resulting in better thermal stability than physical blending. A DSC analysis confirmed the glass transition temperatures (Tgs) of different samples, verifying that incorporating SiO_2 through copolymerization effectively delayed the Tgs. The results from the universal testing indicate that all blending methods effectively improved

the mechanical properties of PMMA/SiO$_2$ composites. The results of UV/Vis scanning and scratching tests reveal that PMMA-*b*-SiO$_2$ provides moderate scratch resistance (4H) and transmittance (85.6%) compared to PMMA. In conclusion, the block copolymerization method for preparing PMMA-*b*-SiO$_2$ preserved the high hardness and transmittance of the original PMMA while maintaining its mechanical strength and improving its thermal stability with only a slight sacrifice in maximum tensile strength. We believe this simple and controllable method can provide a new perspective regarding various polymers and fillers, making it suitable for applications in thermal insulation materials.

Author Contributions: C.-K.L.: Investigation, Methodology, Data curation; J.-W.X.: Investigation, Methodology, Writing—original draft; P.-J.T.: Writing—original draft, Funding acquisition; H.-Y.W.: Data curation, Writing—original draft; Z.-W.L.: Writing—original draft; T.-Y.L.: Investigation, Conceptualization; C.-Y.K.: Conceptualization, Funding acquisition, Supervision, Project administration, Writing—review and editing. All authors have read and agreed to the published version of the manuscript.

Data Availability Statement: Dataset available on request from the authors.

Conflicts of Interest: The authors declare no conflict of interest.

References

1. Boz, Z. Packaging. In *Encyclopedia of Food Safety*, 2nd ed.; Smithers, G.W., Ed.; Academic Press: Oxford, UK, 2024; pp. 631–647. [CrossRef]
2. Yadav, R.; Singh, M.; Shekhawat, D.; Lee, S.-Y.; Park, S.-J. The role of fillers to enhance the mechanical, thermal, and wear characteristics of polymer composite materials: A review. *Compos. Part A Appl. Sci. Manuf.* **2023**, *175*, 107775. [CrossRef]
3. Bommegowda, K.B.; Renukappa, N.M.; Rajan, J.S. *Role of Fillers in Controlling the Properties of Polymer Composites: A Review*; Springer International Publishing: Cham, Switzerland, 2021; pp. 637–648.
4. Van de Werken, N.; Tekinalp, H.; Khanbolouki, P.; Ozcan, S.; Williams, A.; Tehrani, M. Additively manufactured carbon fiber-reinforced composites: State of the art and perspective. *Addit. Manuf.* **2020**, *31*, 100962. [CrossRef]
5. Zheng, X.; Ryeon Kim, B.; Joo Hong, S.; Lee, J.-G.; Woo Park, C. Heat transfer analysis of carbon fiber-reinforced corrugated polymer plate heat exchangers. *Appl. Therm. Eng.* **2024**, *244*, 122684. [CrossRef]
6. Liu, J.; Huang, X.; Ren, Y.; Wong, L.M.; Liu, H.; Wang, S. Galvanic corrosion protection of Al-alloy in contact with carbon fibre reinforced polymer through plasma electrolytic oxidation treatment. *Sci. Rep.* **2022**, *12*, 4532. [CrossRef]
7. Luo, G.-M.; Liang, C.-H. Strength Verification of a Carbon-fibre-reinforced Plastic Patch Used to Repair a Cracked Aluminium Alloy Plate. *Appl. Compos. Mater.* **2024**, *31*, 265–289. [CrossRef]
8. Pandiaraj, V.; Ramkumar, P.; Tharik, J.M.; Vikram, R.; Logasubramani, S.; Vivek, C.M. Chemical resistance and mechanical characteristic evaluation of glass fiber reinforced plastic (GFRP) and hybrid natural composites. *Interactions* **2024**, *245*, 173. [CrossRef]
9. Beck, R.; Prewitz, M. Experimental investigation of tensile properties of glass capillary hybridized carbon fiber reinforced plastic (GCRP) for structurally integrated hydrogen storage. *Int. J. Hydrogen Energy* **2024**, *62*, 321–330. [CrossRef]
10. Panpho, P.; Charoonsuk, T.; Vittayakorn, N.; Bongkarn, T.; Sumang, R. Flexible hybrid piezo/triboelectric energy harvester based on a lead-free BNT-BT-KNN ceramic-polymer composite film. *Ceram. Int.* **2024**. [CrossRef]
11. Monia, T.; Ridha, B.C. Polymer-ceramic composites for bone challenging applications: Materials and manufacturing processes. *J. Thermoplast. Compos. Mater.* **2024**, *37*, 1540–1557. [CrossRef]
12. Pavlyuchkova, E.A.; Malkin, A.Y.; Kornev, Y.V.; Simonov-Emel'yanov, I.D. Distribution of Filler in Polymer Composites. Role of Particle Size and Concentration. *Polym. Sci. Ser. A* **2024**, *66*, 113–120. [CrossRef]
13. Akhyar; Gani, A.; Ibrahim, M.; Ulmi, F.; Farhan, A. The influence of different fiber sizes on the flexural strength of natural fiber-reinforced polymer composites. *Results Mater.* **2024**, *21*, 100534. [CrossRef]
14. Albdiry, M. Effect of melt blending processing on mechanical properties of polymer nanocomposites: A review. *Polym. Bull.* **2024**, *81*, 5793–5821. [CrossRef]
15. Ali, Z.; Yaqoob, S.; Yu, J.; D'Amore, A. Critical review on the characterization, preparation, and enhanced mechanical, thermal, and electrical properties of carbon nanotubes and their hybrid filler polymer composites for various applications. *Compos. Part C Open Access* **2024**, *13*, 100434. [CrossRef]

16. Liu, T.; Zhong, J. Effect of Dispersion of Nano-inorganic Particles on the Properties of Polymer Nanocomposites. *IOP Conf. Ser. Mater. Sci. Eng.* **2019**, *563*, 022026. [CrossRef]
17. Fu, S.-Y.; Feng, X.-Q.; Lauke, B.; Mai, Y.-W. Effects of particle size, particle/matrix interface adhesion and particle loading on mechanical properties of particulate–polymer composites. *Compos. Part B Eng.* **2008**, *39*, 933–961. [CrossRef]
18. Bahramnia, H.; Semnani, H.M.; Habibolahzadeh, A.; Abdoos, H. Epoxy/polyurethane hybrid nanocomposite coatings reinforced with MWCNTs and SiO$_2$ nanoparticles: Processing, mechanical properties and wear behavior. *Surf. Coat. Technol.* **2021**, *415*, 127121. [CrossRef]
19. Tao, J.; Dong, L.; Wu, Y.; Liu, X.; Xie, J.; Wu, H.; Ran, Q. Fabrication of room temperature self-healing, robust superhydrophobic coatings via spraying dual cross-linking supramolecular silicone polymer/SiO$_2$ composite. *Compos. Part B Eng.* **2024**, *273*, 111245. [CrossRef]
20. Made Joni, I.; Vanitha, M.; Panatarani, C.; Faizal, F. Dispersion of amorphous silica nanoparticles via beads milling process and their particle size analysis, hydrophobicity and anti-bacterial activity. *Adv. Powder Technol.* **2020**, *31*, 370–380. [CrossRef]
21. Zhao, Z.; Liang, N.; Shimizu, T.; Shingubara, S.; Ito, T. Antifouling performance against SiO$_2$ particulate matter adhesion of Cyclo Olefin Polymer nanopillar surfaces. *Environ. Sci. Nano* **2024**. [CrossRef]
22. El Far, B.; Rizvi, S.M.M.; Nayfeh, Y.; Shin, D. Investigation of heat capacity and viscosity enhancements of binary carbonate salt mixture with SiO$_2$ nanoparticles. *Int. J. Heat Mass Transf.* **2020**, *156*, 119789. [CrossRef]
23. Jeon, J.G.; So, B.J.; Choi, Y.; Han, Y.; Kim, T.; Shin, G.; Lee, J.H.; Kim, H.J.; Kim, J.H.; Farhangdoust, S.; et al. Thermo-mechanical properties of shape-recoverable structural composites via vacuum-assisted resin transfer molding process and in-situ polymerization of poly (tert-butyl acrylate-co-acrylic acid) copolymer. *Compos. Part A Appl. Sci. Manuf.* **2024**, *185*, 108360. [CrossRef]
24. Formon, G.J.M.; Jayaratnam, J.; Guibert, C.; Van Zee, N.J.; Nicolaÿ, R. Cross-Linking Vitrimers after Melt Processing Using Supramolecularly Masked Dynamic Cross-Linkers. *Macromolecules* **2024**, *57*, 8277–8286. [CrossRef]
25. Feng, T.; Xu, P.; Wang, Y.; Gao, Y.; Wang, H.; Dong, J.; Peng, H.-X.; Qin, F. Magnetic fiber enabled curing electrogram: Real-time process monitoring for thermosetting polymer materials. *Compos. Sci. Technol.* **2022**, *227*, 109598. [CrossRef]
26. Alghamdi, M.N. Thermoplastic composite system using polymer blend and fillers. *J. King Saud Univ. Eng. Sci.* **2022**, *34*, 361–365. [CrossRef]
27. Tavakoli, M.; Bakhtiari, S.S.E.; Karbasi, S. Incorporation of chitosan/graphene oxide nanocomposite in to the PMMA bone cement: Physical, mechanical and biological evaluation. *Int. J. Biol. Macromol.* **2020**, *149*, 783–793. [CrossRef] [PubMed]
28. Merajikhah, A.; Soleimani, M. Bone Cement and Occupational Hazards for Healthcare Providers and Patients: A Narrative Review. *Curr. Surg. Rep.* **2024**, *12*, 252–259. [CrossRef]
29. Wan, Z.; Gao, Y.; Wang, Y.; Zhang, X.; Gao, X.; Zhou, T.; Zhang, Z.; Li, Z.; Lin, Y.; Wang, B.; et al. High-purity butoxydibutylborane catalysts enable the low-exothermic polymerization of PMMA bone cement with enhanced biocompatibility and osseointegration. *J. Mater. Chem. B* **2024**, *2*, 8911–8918. [CrossRef]
30. Wang, X.-D.; Shen, Z.-X.; Sang, T.; Cheng, X.-B.; Li, M.-F.; Chen, L.-Y.; Wang, Z.-S. Preparation of spherical silica particles by Stöber process with high concentration of tetra-ethyl-orthosilicate. *J. Colloid Interface Sci.* **2010**, *341*, 23–29. [CrossRef]
31. Young, J.B.; Hughes, R.W.; Tamura, A.M.; Bailey, L.S.; Stewart, K.A.; Sumerlin, B.S. Bulk depolymerization of poly(methyl methacrylate) via chain-end initiation for catalyst-free reversion to monomer. *Chem* **2023**, *9*, 2669–2682. [CrossRef]
32. Kashiwagi, T.; Inaba, A.; Brown, J.E.; Hatada, K.; Kitayama, T.; Masuda, E. Effects of weak linkages on the thermal and oxidative degradation of poly(methyl methacrylates). *Macromolecules* **1986**, *19*, 2160–2168. [CrossRef]
33. Zhan, Y.; Nan, B.; Liu, Y.; Jiao, E.; Shi, J.; Lu, M.; Wu, K. Multifunctional cellulose-based fireproof thermal conductive nanocomposite films assembled by in-situ grown SiO$_2$ nanoparticle onto MXene. *Chem. Eng. J.* **2021**, *421*, 129733. [CrossRef]
34. Bee, S.-L.; Abdullah, M.A.A.; Mamat, M.; Bee, S.-T.; Sin, L.T.; Hui, D.; Rahmat, A.R. Characterization of silylated modified clay nanoparticles and its functionality in PMMA. *Compos. Part B Eng.* **2017**, *110*, 83–95. [CrossRef]
35. Li, Y.; Zhao, X.; Li, D.; Zuo, X.; Yang, H. Multifunctional composite phase change materials: Preparation, enhanced properties and applications. *Compos. Part A Appl. Sci. Manuf.* **2024**, *185*, 108331. [CrossRef]
36. Yuan, M.; Huang, D.; Zhao, Y. Development of Synthesis and Application of High Molecular Weight Poly(Methyl Methacrylate). *Polymers* **2022**, *14*, 2632. [CrossRef]